Journal of the Brazilian Society of Mechanical Sciences and Engineering (2018) 40:529
https://doi.org/10.1007/s40430-018-1443-7

TECHNICAL PAPER

Bifurcation and chaos analysis for a spur gear pair system with friction

Yan Xia[1,2] · **Yi Wan**[1,2] · **Zhanqiang Liu**[1,2]

Received: 2 June 2018 / Accepted: 3 October 2018 / Published online: 20 October 2018

Abstract
Considering time-varying meshing stiffness, gear backlash, static transmission error and tooth face friction, a nonlinear dynamic model for a spur gear pair is proposed to research systematically the dynamic behaviors of system, in which the meshing stiffness of gear pair is deduced and calculated in terms of the extending period method. Meanwhile, the sliding friction force under single-tooth and double-tooth meshing regions is constructed as a function of the meshing principle. Based on the developed model, the bifurcation and chaos characteristics of system under lightly and heavily loaded conditions are studied, respectively, by applied Runge–Kutta numerical method, and the parametric effects of rotational speed, damping ratio and gear backlash on the dynamic behaviors are investigated detailedly. Bifurcation diagram, three-dimensional frequency spectrum, time-domain waveform, frequency plot, phase diagram, Poincaré map and dynamic load are used to discuss and determine motion states and dynamic responses of system. The numerical results represent that with the change of control parameters the system undergoes various types of motion states under different loaded conditions. The corresponding meshing contact states of tooth pair are transformed among no impact, single-sided impact and double-sided impact. The research results can provide certain guidance for choosing suitable parameter values to reduce the amplitude of vibration and even avoid the chaotic response in gear system.

Keywords Gear pair system · Nonlinear dynamics · Tooth face friction · Bifurcation · Chaos · Dynamic load

1 Introduction

Gear system is widely applied in various machineries as power transmission equipment, whose dynamic performance directly affects the stability of system. However, the nonlinear factors consisting of the static transmission error, meshing stiffness, tooth face friction, gear backlash and so forth, are prone to deteriorating vibration response of gear pair, which may cause the system to become unpredictable and uncontrollable. Thus, it is of importance to determine accurately the dynamic characteristics of gear set for avoiding serious vibration and ensuring the running stability of machinery [1, 2].

To improve the dynamic performance of gear transmission system, a sea of studies have been carried out in recent decades. Kahraman and Singh [3–5] simplified the gear system to the mathematical models with single degree of freedom (single DOF) or multi-DOF and then analyzed the dynamic behaviors of system with the effect of clearance and meshing stiffness. Raghothama and Narayanan [6] investigated the periodic and chaotic motions in gear–rotor–bearing system by adopting the incremental harmonic balance method (IHBM) and numerical simulation method. Theodossiades and Natsiavas [7] used the analytical methodology to research the dynamics of a gear pair system with backlash and time-dependent mesh stiffness and then verified the obtained results by numerical calculation. The influences of meshing damping, amplitude of meshing stiffness and static torque on dynamic characteristic of two gear pairs were described by Al-Shyyab and Kahraman [8, 9]. Then, Shen et al. [10] derived a system model of a spur gear pair with single-DOF, in which the influences of damping ratio and the excitation amplitude on system response were analyzed by using IHBM. Likewise, to determine the effect of backlash on dynamic characteristics in two-stage gear system,

Technical Editor: Pedro Manuel Calas Lopes Pacheco, D.Sc.

✉ Yi Wan
wanyi@sdu.edu.cn

[1] Key Laboratory of High Efficiency and Clean Mechanical Manufacture, Ministry of Education, School of Mechanical Engineering, Shandong University, Jinan, China

[2] National Demonstration Center for Experimental Mechanical Engineering Education, Shandong University, Jinan, China

Walha et al. [11] developed a torsional dynamic model and used Newton–Raphson algorithm to obtain the dynamic behaviors of system. Considering the nonlinear suspension, Chang-Jian [12] studied the dynamic response of a gear–bearing system, which demonstrated the motion forms of the system by using nonlinear dynamic analysis method. In Refs. [13, 14], Melnikov analytical method was applied by Farshidianfar and Saghafi to predict the key values of system parameter for the occurrence of homoclinic bifurcation and onset of chaos. With the aim to obtain the torsional dynamic behaviors of wind turbine gearbox, Zhao and Ji [15] built a nonlinear dynamic model under the internal and external excitations and thus the influences of excitation parameters on the dynamic responses of system were investigated through a numerical integration method. Wang et al. [16] proposed a three-DOF torsional dynamic model of the locomotive traction system to carry out the dynamic analysis. The dynamic behaviors of system were identified and described by time-domain response diagram, phase plane diagram, Poincaré map and bifurcation diagram. In addition, Gou et al. [17] modified a dynamic model of a gear system to analyze the influence of flash temperature on the dynamic responses of system, in which the temperature stiffness was constructed and considered into the mathematical model. The analysis result confirmed that the developed method of the flash temperature is useful. For the purpose of investigating the relationship between backlash and bearing clearance, Liu et al. [18] considered several kinds of forces such as the backside contact force, bearing forces and shift of the bearing position in the model, where the detailed research was carried out in quasi-static and dynamic analyses.

Considering the effect of friction on the dynamic features of the gear system, Howard et al. [19] established a dynamic model with 16-DOF and simulated the dynamic behaviors under different working conditions. Vaishya and Singh [20] presented a dynamic model of a gear pair with meshing stiffness, damping and tooth face friction. Then, they [21] analyzed further the effect of the strong nonlinearity caused by sliding friction on the system and discussed the dynamic behaviors to the change of key parameters. Several sliding friction formulations applied in the spur gear system are examined and compared in the influence on the dynamic response in Ref [22]. Subsequently, Wang et al. [23] investigated and compared the nonlinear phenomena in a gear pair with the friction and non-friction and obtained the crucial differences in the system behavior. Considering meshing stiffness, backlash and friction, Chen et al. [24] provided a dynamic model for a gear pair system with multi-DOF and predicted the motion states. Based on the model above, Moradi [25] studied the nonlinear oscillations with the backlash nonlinearity, and confirmed the dynamic responses of the system consisting of primary, super-harmonic and sub-harmonic resonances by using the multiple scale method. Xiang et al. [26] built a six-DOF mathematical model of a spur gear pair with surface friction and used the support stiffness and rotational speed as control parameters to analyze the nonlinear dynamic features. Based on a quasi-static wear model and a translational–rotational-coupled nonlinear dynamic model, Liu et al. [27] developed a wear prediction method to describe the relationship between surface wear and dynamic responses of system. The numerical results revealed that the interaction relation between the above two is strong. A six-DOF model of gear pair under friction–vibration interactions was built by Jiang and Liu [28], in which the dynamic responses of system with sliding friction were obtained. Wang et al. [29] presented a dynamic model for locomotive gear transmission system with tooth surface and performed the investigation for the influence of tooth surface friction on the parametric vibration stability. Zhou et al. [30] proposed a gear–rotor–bearing model with 16-DOF, which took into consideration friction force, gravity, eccentricity and so on, and studied the influences of mean load and friction coefficient on the dynamic behaviors using numerical integration method. The corresponding results indicated that the friction force could increase the vibration amplitude of system.

From above, a multitude of works have investigated the nonlinear dynamics with and without frictional force, respectively. Nevertheless, the dynamic model with the frictional force in some references should be improved. It is due to the deficiency that only the frictional force under single-tooth meshing area is considered. Additionally, the meshing force is assumed to be uniform distribution between the tooth pairs when the frictional force under double-tooth meshing area is considered in the gear system. Overcoming the two shortcomings above, the influence of frictional force on the dynamic response of gear system can be more factually reflected based on the proposed dynamic model. Rotational speed, damping ratio and meshing backlash as control parameters are used to research the dynamic characteristics of the gear system in detail. Meantime, the nonlinear dynamic behaviors of the system are discussed utilizing time-domain waveform diagram, frequency plot, phase portrait, Poincaré map and dynamic load diagram.

The structure of the study is organized into four sections. The dynamic model and equation of motion for a spur gear pair system are presented in Sect. 2, where the nonlinearity of friction factor and time-varying meshing stiffness are described as well. In Sect. 3, the equation of motion for the system is solved by numerical method and then bifurcation and chaos features with different bifurcation parameters are investigated. Finally, some brief conclusions are drawn from the research in Sect. 4.

2 Description of dynamic model for a spur gear pair system

2.1 Time-varying meshing stiffness

In order to ensure the steady gear transmission, the meshing coincidence degree of gears ε is not generally an integer, which is under the range of 1–2. Therefore, the alternation meshing between single tooth and double teeth occurs, leading to the change of meshing stiffness periodically. When calculating the meshing stiffness, only the abrupt changes caused by the single-tooth meshing and double-tooth meshing alternately are taken into account in many researches. However, the change of the stiffness of the tooth itself with the movement of the meshing point is neglected. The way to deal with meshing stiffness may result in large error and cannot reflect the actual situation of gear meshing. Based on the previous research [26], the extending period method is thus introduced to calculate the time-varying meshing stiffness so as to analyze conveniently and accurately the meshing situation and the dynamic meshing force between the meshing teeth.

Figure 1 presents the meshing schematic diagram of the spur gear pair. In Fig. 1a, r_{ai} and r_{bi} are the radius of addendum circle and base circle of the gear system, respectively. ω_i denotes the rotational speed of the gear i ($i=1$, 2), respectively. N_2 and N_1 are the starting point and ending point of theoretical meshing line, respectively. It is assumed that the gear pair starts meshing in point B_2 and moves along the meshing line N_1N_2 to the point B_1 out of contact. From Fig. 1b, it can be seen in the moving distance N_1N_2 of the meshing points that B_2K_2 and K_1B_1 are double-tooth meshing areas and K_1K_2 is the single-tooth meshing area, respectively.

The situation of gear meshing is expanded in time axis, as shown in Fig. 2. Here, $T_m=2\pi/z_1\omega_1=2\pi/z_2\omega_2$ is the meshing

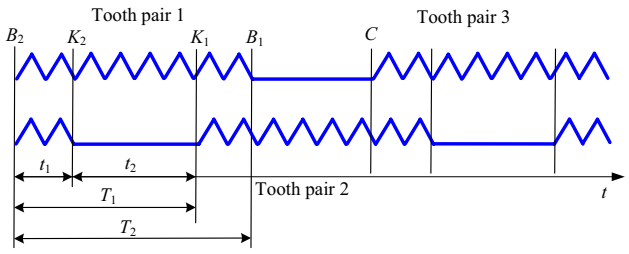

Fig. 2 Sketch of mesh stiffness extending on meshing time

period. T_1 is equal to T_m, where T_1 represents the time that the meshing point moves a basic pitch P_n along the meshing line. According to the definition of mesh coincidence degree, $\varepsilon=B_1B_2/P_n$. Hence, $T_2=\varepsilon\cdot T_m$, in which T_2 is the time that the meshing point moves from point B_2 to point B_1. In addition, t_1 refers to the time that the meshing point is under the double-tooth meshing area. Likewise, t_2 shows the time that the meshing point is in the single-tooth meshing area. In time domain, the meshing gear pair can be divided into odd meshing gear pair and even meshing gear pair. It can be found from the Fig. 2 that the time interval between the two odd meshing gear pairs or two even meshing gear pairs is $2T_1$. For instance, the meshing point moves from point B_2 to point C, and in the time process, tooth pair 1 is out of meshing and tooth pair 3 starts to be in meshing. However, it clearly shows that the tooth pair 1 does not involve in the meshing when it moves from B_1 to C, which means that the meshing stiffness is zero. Therefore, the time-varying meshing stiffness of odd meshing gear with the period $2T_1$ can be expressed as follows:

$$k_1(t)=\begin{cases} k(t) & 0<t<T_2 \\ 0 & T_2<t<2T_1 \end{cases} \tag{1}$$

Similarly, the period of even meshing gear pair is also $2T_1$, in which the meshing stiffness of even meshing gear

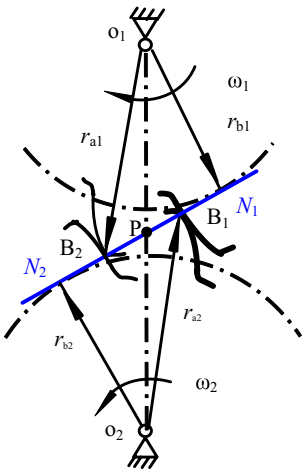

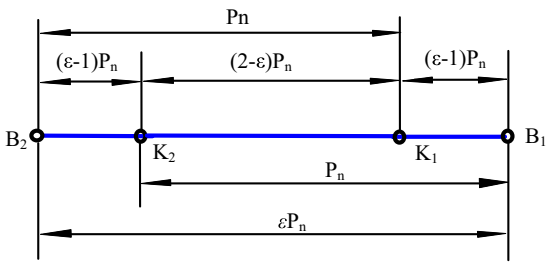

Fig. 1 Schematic illustration of meshing between the gear pairs. **a** Sketch of meshing at the end surface of gears. **b** Physical interpretation of meshing coincidence degree

pair can be written as $k_2(t) = k_1(t + 2T_1)$. Therefore, when the gear backlash is $2b_c$, the elastic restoring force F_{ki}, i.e., the dynamic load of the gear transmission [31], is defined as follows:

$$F_{ki} = k_i(t) \cdot f(x) \quad (i = 1, 2) \tag{2}$$

where $f(x)$ refers to the nonlinear backlash function which could adopt the following expression:

$$f(x) = \begin{cases} x - b_c, & x > b_c \\ 0, & |x| \le b_c \\ x + b_c, & x < -b_c \end{cases} \tag{3}$$

Here, b_c is half of the tooth backlash and x is the total relative elastic deformation.

According to the nonlinear backlash function $f(x)$ in Fig. 3, there are three impact states consisting of no impact (state I), single-sided impact (state II) and double-sided impact (state III) in a gear system [2, 3]. From Fig. 3, when x is in the range of $x_{\min} > b_c$ or $x_{\max} < -b_c$, there is no tooth separation where the gear system shows no impact in state I. It means that the dynamic load F_{ki} is always greater than zero. Then, when x is at $x_{\max} > b_c$ and $x_{\min} > -b_c$ or $x_{\max} < b_c$ and $x_{\min} < -b_c$, the gear system has single-sided impact in state II, in which the dynamic load F_{ki} would have zero value but wll not have negative values. Additionally, the double-sided impact (state III) will occur in the gear system when x is in the range of $x_{\min} < -b_c$ and $x_{\max} > b_c$. The corresponding F_{ki} will have negative values.

The damping force can be defined as

$$F_{ci} = c_{mi} \cdot \dot{x} \tag{4}$$

where c_{mi} denotes the meshing damping for the gear pair i ($i = 1, 2$).

Hence, the dynamics meshing force can be written as:

$$F_i = F_{ki} + F_{ci} \quad (i = 1, 2) \tag{5}$$

2.2 Nonlinearity of friction factor

Based on the actual situation of gear meshing, the relative sliding velocity direction of the tooth surface for the meshing gear pair is opposite around the pitch circle. Meantime, the meshing force of the tooth surface changes with the movement of meshing point. Hence, the direction of the frictional force at the pitch could be changed abruptly by the above reasons. The point that the tooth pair 1 in Fig. 2 starts to enter meshing is selected as a starting point. Thus, the direction coefficient of sliding friction force of tooth surface can be expressed with period $2T_1$ as follows:

$$\lambda_i = \begin{cases} 1 & 0 < t < t_2 \\ -1 & t_2 < t < T_2 \\ 0 & T_2 < t < 2T_1 \end{cases} \quad (i = 1, 2) \tag{6}$$

As a function of the Coulomb's law of friction, the magnitude of the frictional force is proportional to the positive pressure. The friction force can be expressed by

$$F_{fi} = \lambda_i \mu F_i \quad (i = 1, 2) \tag{7}$$

where μ represents the coefficient of friction and F_i is the dynamics meshing load.

In terms of gear geometry in Fig. 1a, the frictional force arms are expressed as follows [32]:

$$\begin{aligned} l_{11}(t) &= (r_{b1} + r_{b2}) \tan\alpha - \sqrt{r_{a2}^2 - r_{b2}^2} + r_{b1}\omega_1 t \\ l_{12}(t) &= (r_{b1} + r_{b2}) \tan\alpha - \sqrt{r_{a2}^2 - r_{b2}^2} + r_{b1}\omega_1 t + P_n = l_{11}(t + T_1) \\ l_{21}(t) &= \sqrt{r_{a2}^2 - r_{b2}^2} - r_{b1}\omega_1 t \\ l_{22}(t) &= \sqrt{r_{a2}^2 - r_{b2}^2} - r_{b1}\omega_1 t + P_n = l_{21}(t + T_1) \end{aligned} \tag{8}$$

where l_{1i} and l_{2i} are the frictional force arms of the tooth pair i ($i = 1, 2$), respectively.

Then, the friction torque of gear i caused by friction force between ith tooth pair can be given by:

$$T_{f1i} = F_{fi} \cdot l_{1i} \quad T_{f2i} = F_{fi} \cdot l_{2i} \quad (i = 1, 2) \tag{9}$$

From the previous analysis, the meshing force, friction force and friction torque between the gear pair are written as:

$$F = \sum_{i=1}^{N} F_i \quad F_f = \sum_{i=1}^{N} F_{fi} \quad T_{f1} = \sum_{i=1}^{N} T_{f1i} \quad T_{f2} = \sum_{i=1}^{N} T_{f2i} \quad (i = 1, 2) \tag{10}$$

where N is the maximum number of pairs of meshing gears and can be obtained as

$$N = \text{ceil}(\varepsilon) \tag{11}$$

Here, ceil(ε) is the smallest integer that is greater than or equal to ε.

2.3 Equations of the gear pair system

The generalized lumped dynamic model with torsional-DOF for a spur gear pair system is provided, ignoring the transverse and axial elastic deformation of the drive shaft and

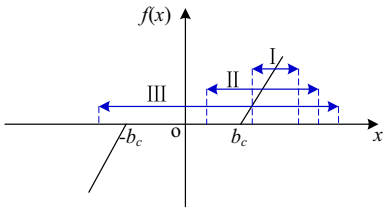

Fig. 3 Backlash nonlinear function

the elastic deformation of the support system, as shown in Fig. 4. For the sake of convenient calculation in the model, it is assumed that the driving and driven gears are standard involute gears. The meshing stiffness and damping parameter are same on the unit tooth width. And the sliding friction factors are equal and constant in the system, neglecting the rolling friction. Here, θ_1 and θ_2 represent the torsional vibration displacement of the driving and driven gears, respectively. I_1 and I_2 show the moment of inertia for the two gears, respectively. m_1 and m_2 mean the equivalent mass of the two gears, respectively. r_{b1} and r_{b2} represent the radius of base circles of the gear system, respectively. T_{in} and T_{ou} are the torques acting on the driving and driven gears, respectively. F_f refers to the sliding friction between the gears. In addition, $k(t)$, c_m, $e(t)$ and $2b_c$ are time-varying meshing stiffness, meshing damping, the static transmission error and gear backlash in the gear pair system, respectively.

According to Newton's laws of motion, the dynamic differential equations of the gear pair system in Fig. 4 can be expressed as follows:

$$\begin{aligned} I_1\ddot{\theta}_1 + r_{b1}F + T_{f1} &= T_{in} \\ I_2\ddot{\theta}_2 - r_{b2}F - T_{f2} &= -T_{ou} \end{aligned} \tag{12}$$

Due to the presence of gear backlash, the gear pair contains a rigid body displacement [33]. To eliminate the rigid body displacement that makes the equation solvable, the relative coordinate x is thus described in the gear system, which can be represented by

$$x = r_{b1}\dot{\theta}_1 - r_{b2}\dot{\theta}_2 - e(t) \tag{13}$$

where $e(t) = e_m + e_r \cdot \sin(\omega t + \varphi)$ refers to the static transmission error, in which e_m is the mean value, e_r represents the volatility value, and φ stands for the initial phase of error.

Substituting the relative coordinate x as a new degree of freedom into Eq. (12), Eq. (12) can then be rewritten as the following expressions:

$$\begin{aligned} &\ddot{x} + \frac{1}{m_e}\left[\eta_1(t) + \eta_2(t)\right]c_m\dot{x} \\ &\quad + \frac{1}{m_e}\left[\eta_1(t)k_1(t) + \eta_2(t)k_2(t)\right]f(x) = \frac{F}{m_e} - \ddot{e}(t) \end{aligned} \tag{14}$$

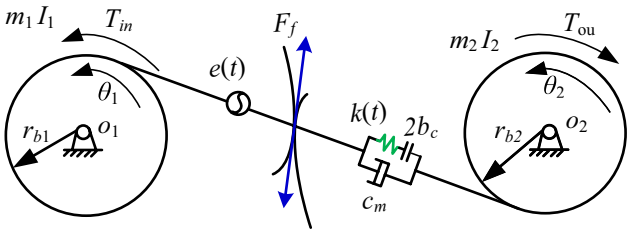

Fig. 4 Dynamic model of a spur gear pair system with sliding friction

where $m_e = 1/(1/m_{e1} + 1/m_{e2})$ shows the equivalent mass of the gear pair. Here, m_{e1} and m_{e2} are the equivalent mass of the driving and driven gears, respectively, which can be obtained by $m_{e1} = I_1/r_{b1}^2$ and $m_{e2} = I_2/r_{b2}^2$. And, $F = T_1/r_{b1} = T_2/r_{b2}$ is the average force caused by external torque. In addition, $\eta_1(t)$ and $\eta_2(t)$ are the period function about frictional force arms, which are written as follows:

$$\begin{aligned} \eta_1(t) &= 1 + m_e\mu\lambda_1\left(\frac{L_{11}}{m_1 r_{b1}} + \frac{L_{12}}{m_2 r_{b2}}\right) \\ \eta_2(t) &= 1 + m_e\mu\lambda_2\left(\frac{L_{21}}{m_1 r_{b1}} + \frac{L_{22}}{m_2 r_{b2}}\right) \end{aligned} \tag{15}$$

In order to improve the accuracy of calculation, Eq. (14) should be transformed with dimensionless form.

Then, the dimensionless parameters $\tau = \omega_n t$ and nominal dimension b_n are introduced, where the system response parameters could be expressed with $x = Xb_n$, $\dot{x} = \dot{X}b_n\omega_n$, $\ddot{x} = \ddot{X}b_n\omega_n^2$ and $\Omega = \omega/\omega_n$. Additionally, the dimensionless nonlinear backlash function $f(X)$ can be described as follows:

$$f(X) = \begin{cases} X - b, & X > b \\ 0, & |X| \le b \\ X + b, & X < -b \end{cases} \tag{16}$$

where $b = b_c/b_n$.

Hence, the dimensionless equation of system can be represented by:

$$\begin{aligned} &\ddot{X} + 2\zeta\left[\eta_1(\tau) + \eta_2(\tau)\right]\dot{X} + \frac{1}{k_m} \\ &\left[\eta_1(\tau)k_1(\tau) + \eta_2(\tau)k_2(\tau)\right]f(X) = F_m + F_a\Omega^2\cos(\Omega\tau + \varphi) \end{aligned} \tag{17}$$

where $\zeta = \frac{c_m}{2m_e\omega_n}$, $F_m = \frac{F}{b_n m_e\omega_n^2}$, $F_a = \frac{e_r}{b_n}$.

In addition, the dimensionless dynamic load can be given by

$$F_k = \frac{1}{k_m}\left[\eta_1(\tau)k_1(\tau) + \eta_2(\tau)k_2(\tau)\right]f(X) \tag{18}$$

3 Numerical simulation and discussion

Owing to the existence of the tooth surface friction, time-varying stiffness, backlash and the static transmission error, the gear system is a complex system with nonlinearity and time variation. To understand comprehensively the dynamic features of system, rotational speed Ω, damping ratio ζ and backlash b are selected as bifurcation parameter to investigate the influences on the system response, in which the corresponding dynamic equations are solved using Runge–Kutta numerical method with the initial conditions $X(0) = 0$ and $\dot{X}(0) = 0$. The dynamic responses of the gear

system with sliding friction can be systematically analyzed from bifurcation diagrams and 3-D frequency spectrum. The main physical parameters of system are listed in Table 1. Besides, when the external load varies, the force ratio F_m/F_a that reflects the carrying capacity of gear transmission system also changes. Apparently, in order to study the effect of F_m and F_a on dynamic behaviors, it is essential to analyze the bifurcation and chaos characteristics under lightly and heavily loaded conditions, respectively [3].

3.1 Model validation

Tooth surface friction force has an evident effect on the dynamic behaviors of the gear system. Thus, a number of literatures have considered the sliding friction factor in the dynamic models, where some models with friction should be perfected owing to the fact that the obtained friction force cannot factually reflect the effect on the vibration of the gear pair system. Therefore, time-domain waveform of the relative coordinate along the line of meshing is illustrated in Fig. 5 to verify the accuracy of the dynamic model for a spur gear pair system with sliding friction in this paper. The contrast between the proposed model and the model in the literatures is first carried out without friction to prove the correctness of the model of this study and, second, performed under friction condition to analyze the difference between models.

When the coefficient of friction μ is zero and the other parameters of the model in Fig. 4 are the same as those in Ref. [5], Fig. 5a explicitly shows that the displacement X is equal to the displacement P in Ref. [5], which means that the built model without friction is equivalent to the model in Ref. [5]. Then, considering the friction factor that the friction coefficient μ is 0.07, the displacement X is larger than the displacement P in Fig. 5b. It clearly indicates that tooth face friction could aggravate the vibration of gear pair, which is in agreement with the research conclusion in Ref. [30]. Besides, the friction force of tooth surface is briefly expressed as the product of the contact force between the gear teeth and friction coefficient in Ref. [29]. Thus, keeping the system parameters same with the above analysis, the displacement Y can be solved as seen in Fig. 5b, in which the method of calculating the friction force in Ref. [29] is adopted. It could be observed that the displacement Y is less than displacement P, which seems to reveal that the friction could suppress the system response. The result is caused by the unreasonable assumptions that the dynamic change of friction force is omitted. Overall, based on the models in the literature, the proposed model with friction force is reasonably improved that can factually reflect the influence of tooth surface friction on gear vibration.

Table 1 Parameters of the gear pair system

Parameters	Value
Number of teeth, z_1/z_2	25
Modulus, m (mm)	5
Mass, m_1/m_2 (kg)	1
Moment of inertia, I_1/I_2 (kg mm^2)	800
Face width, B (mm)	60
Pressure angle, α (°)	20

3.2 Effect of rotational speed Ω on bifurcation and chaos characteristics

Rotational speed Ω is one of the main physical parameters for the gear transmission system. Thus, Ω is chosen as a control parameter to investigate the influence on the bifurcation and chaos feature of system. Meanwhile, the other system parameters are listed as follows: friction coefficient $\mu = 0.07$, damping ratio $\zeta = 0.07$, gear backlash $b = 1$, force ratio $F_m/F_a = 0.5$ or 2; namely, the gear system is under lightly or heavily loaded condition. Figures 6 and 7 show the bifurcation diagrams and three-dimensional (3-D) spectrum programs with the varying rotational speed Ω under different loaded conditions. From these figures, when Ω increases, the system presents complex motion forms, including period motion, i.e., period-one and multi-period motions, chaotic motion and so on. Specifically, comparing Fig. 6a with Fig. 6b, it can be clearly found that the system undergoes the wider region of chaotic motion under the condition of light load than that under the condition of heavy load, where the chaos is nearly replaced by period motion under the condition of heavy load. The phenomenon can be inspected from the corresponding 3-D spectrum programs in Fig. 7. Chaotic

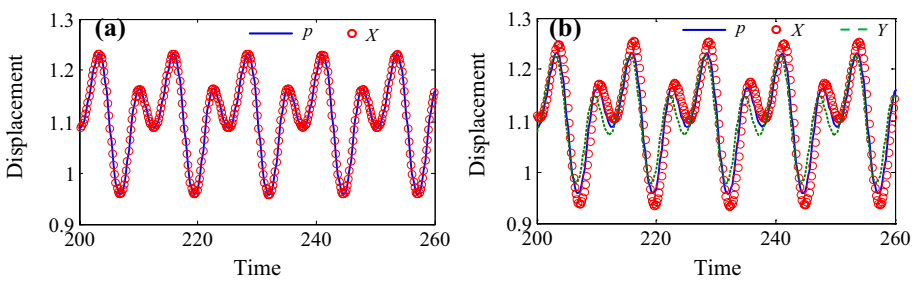

Fig. 5 Time-domain waveform. **a** Without friction; **b** with friction coefficient $\mu = 0.07$

motion always means that the system is under the unstable and uncontrollable state. It could be concluded that the stable motion occupies the dominant position under the heavily loaded condition, in which there is similar conclusion in Ref. [5].

In order to clearly reveal the motion states under lightly loaded condition, time-domain waveform, frequency plot, phase diagram, Poincaré map and dynamic load curve are used to demonstrate the dynamic features of system from Figs. 8, 9, 10, 11, 12, 13, 14, 15, 16 and 17. In the range of $\Omega < 0.78$, the gear pair keeps in the period-one state. Under $\Omega = 0.3$, the time-domain waveform is a single periodic sinusoid, frequency plot possesses an obvious amplitude peak, the phase diagram is an approximate ellipse, and there is only a point in the Poincaré map, as shown in Fig. 8a–c. These reveal that the system is in period-one state. The dynamic load in Fig. 8d is always greater than zero, which demonstrates the meshing gear pairs are in no impact state (state I). In other words, there cannot appear separation between the meshing teeth, which also represents the system is under the stable state. Although jump discontinuity phenomena appears when $\Omega = 0.61$, the motion form of the gear system does not change in Fig. 6a. As Ω increases, the system response changes from

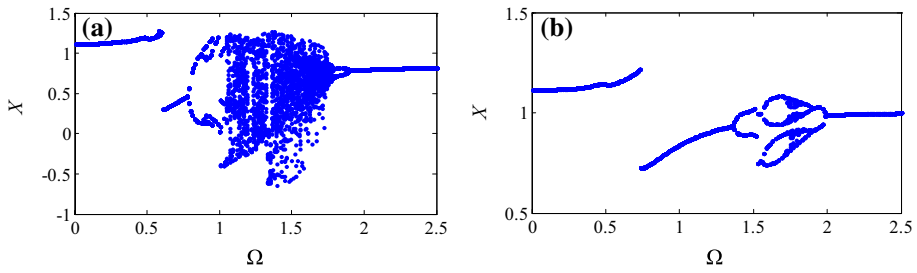

Fig. 6 Bifurcation diagrams with the varying of Ω under lightly and heavily loaded conditions, respectively

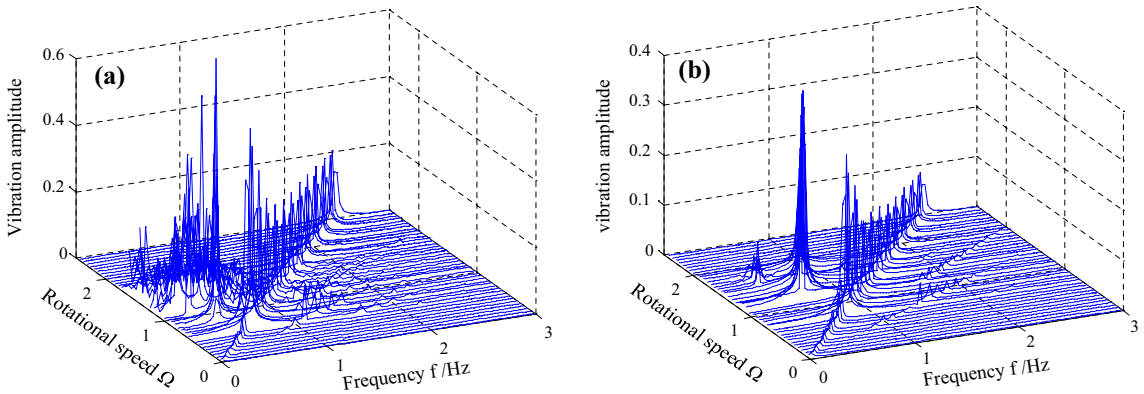

Fig. 7 3-D frequency spectrum with the varying of Ω under lightly and heavily loaded conditions, respectively

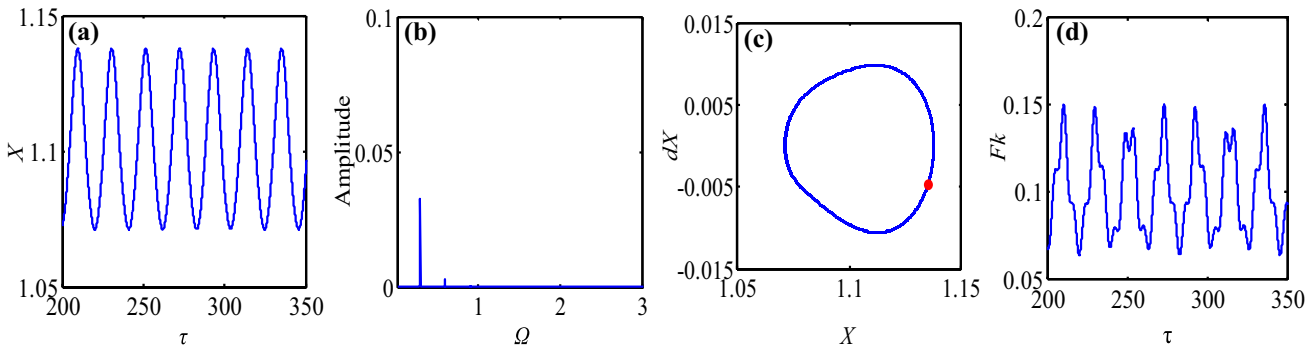

Fig. 8 Dynamic response curves at $\Omega = 0.3$. **a** Time-domain waveform, **b** frequency plot, **c** phase diagram and Poincaré map, **d** dynamic load curve

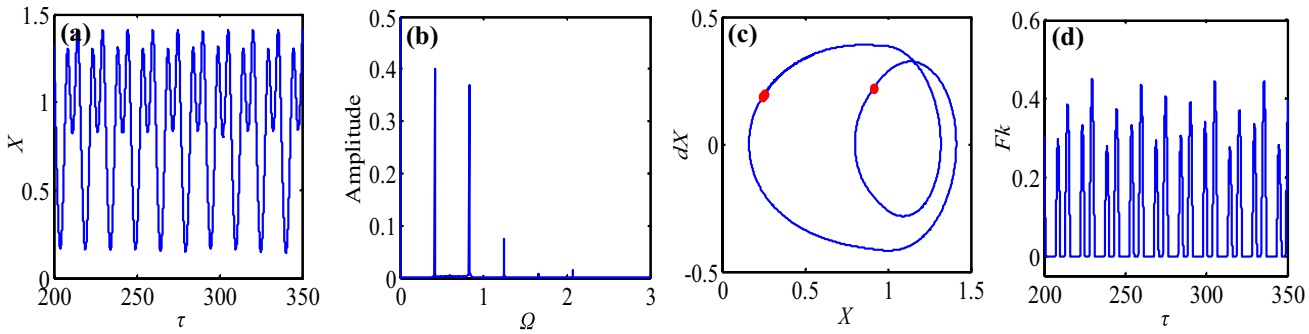

Fig. 9 Dynamic response curves at $\Omega = 0.83$. **a** Time-domain waveform, **b** frequency plot, **c** phase diagram and Poincaré map, **d** dynamic load curve

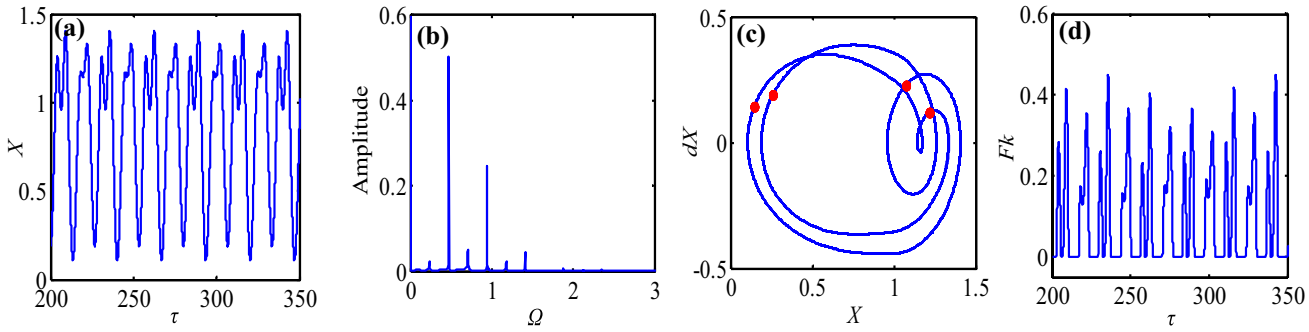

Fig. 10 Dynamic response curves at $\Omega = 0.941$. **a** Time-domain waveform, **b** frequency plot, **c** phase diagram and Poincaré map, **d** dynamic load curve

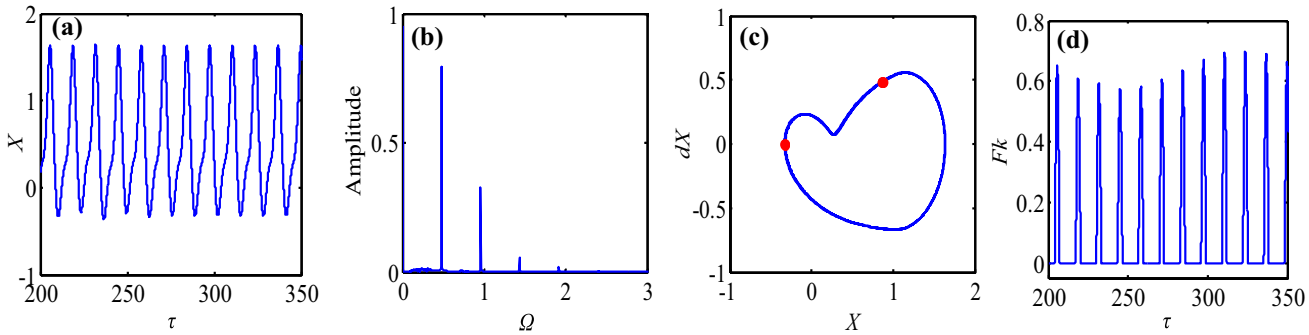

Fig. 11 Dynamic response curves at $\Omega = 0.958$. **a** Time-domain waveform, **b** frequency plot, **c** phase diagram and Poincaré map, **d** dynamic load curve

period-one to period-two motion. Meantime, the meshing state of gear pair transforms from no impact to single-sided impact state. Choosing $\Omega = 0.83$, frequency plot in Fig. 9 comes out demultiplication frequency component, namely 0.5Ω and 1.5Ω. And the meshing gear pair is in state between no impact state and single-sided impact state alternately in Fig. 8d due to the discontinuous presence of dynamic load $F_k = 0$. Besides, single-sided impact state represents a repeated state that the meshing gear contact, separate, re-contact only on the positive tooth surface, which reveals the instability of the system. By increasing the rotational speed Ω further, the gear pair keeps under the single-sided impact state and the dynamic load F_k increases gradually at $0.83 < \Omega < 1.04$. Furthermore, the system response switches between period-two and period-four motions twice, which can be observed in

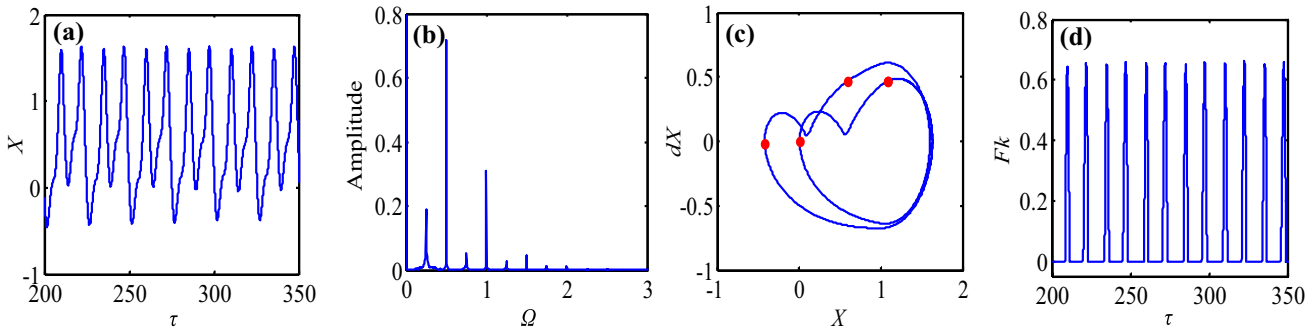

Fig. 12 Dynamic response curves at $\Omega = 1.0$. **a** Time-domain waveform, **b** frequency plot, **c** phase diagram and Poincaré map, **d** dynamic load curve

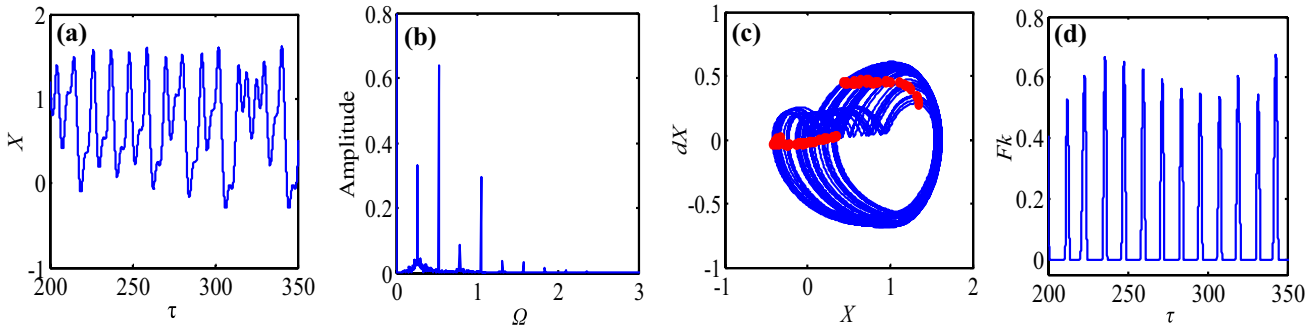

Fig. 13 Dynamic response curves at $\Omega = 1.05$. **a** Time-domain waveform, **b** frequency plot, **c** phase diagram and Poincaré map, **d** dynamic load curve

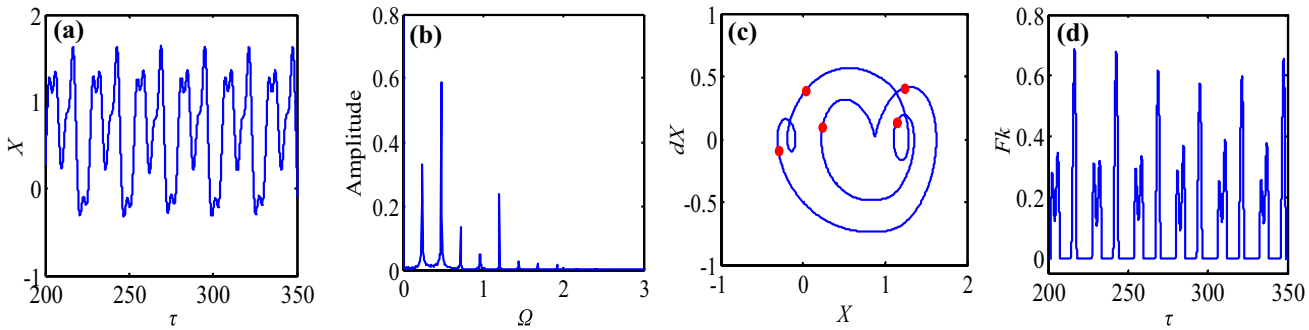

Fig. 14 Dynamic response curves at $\Omega = 1.2$. **a** Time-domain waveform, **b** frequency plot, **c** phase diagram and Poincaré map, **d** dynamic load curve

Figs. 9, 10, 11 and 12. Then, Ω keeps increasing even further, the system starts into chaotic motion. For instance, at $\Omega = 1.05$, there appear continuous frequency components in frequency spectrum diagram, the phase diagram is disorder, and a great deal of discrete points evolved into two fractal structures exist in the Poincaré map in Fig. 13, which shows the characteristics of chaos. Before entering the next chaotic window, gear pair experiences a narrow region of period-five motion. As shown in Fig. 14, under $\Omega = 1.2$, the time-domain waveform is a periodic motion and the Poincaré map has five discrete points, revealing that the system is under period-five motion state. Then, the system goes into the chaos once more. Likewise, when $\Omega = 1.5$, Fig. 15 displays the chaotic behavior of system. Even though system is in chaotic motion under the above two values, the fractal part from Fig. 15c is different with

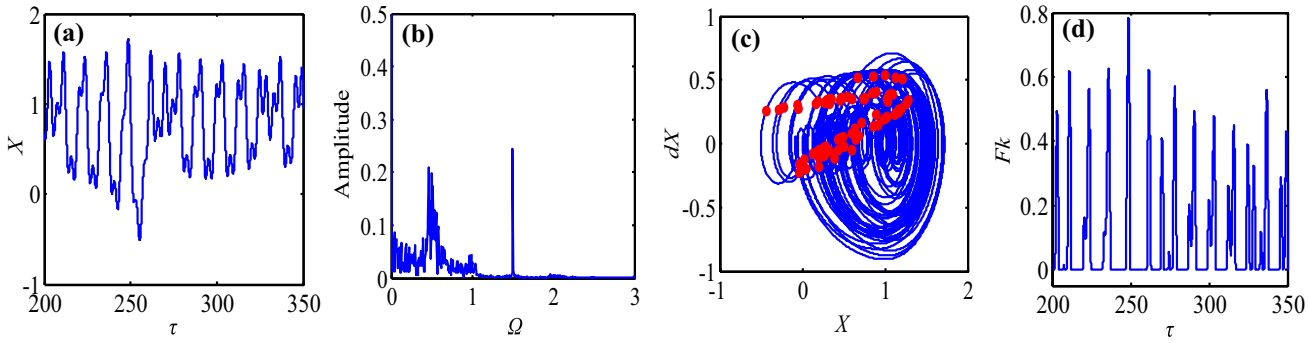

Fig. 15 Dynamic response curves at $\Omega = 1.5$. **a** Time-domain waveform, **b** frequency plot, **c** phase diagram and Poincaré map, **d** dynamic load curve

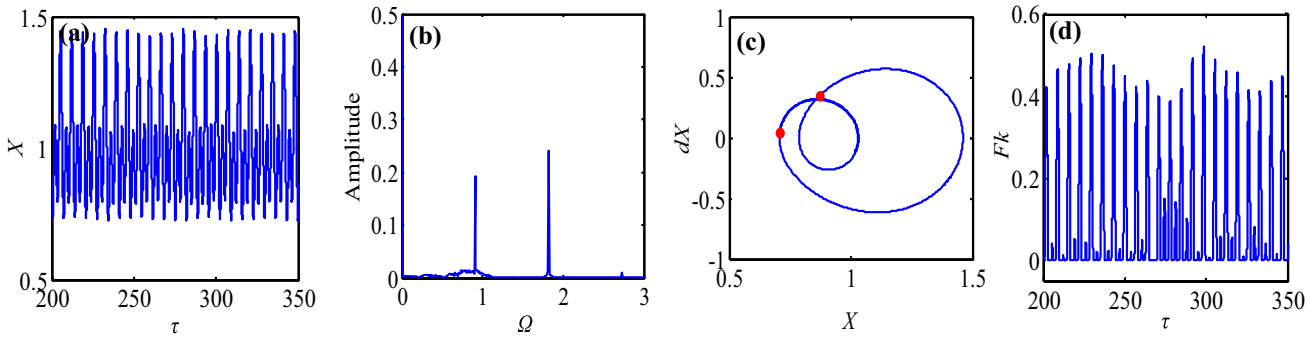

Fig. 16 Dynamic response curves at $\Omega = 1.82$. **a** Time-domain waveform, **b** frequency plot, **c** phase diagram and Poincaré map, **d** dynamic load curve

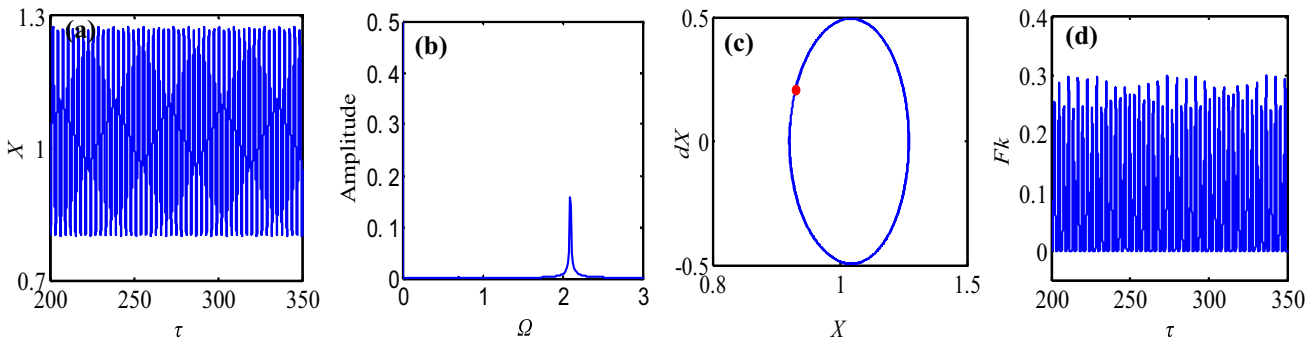

Fig. 17 Dynamic response curves at $\Omega = 2.1$. **a** Time-domain waveform, **b** frequency plot, **c** phase diagram and Poincaré map, **d** dynamic load curve

that in Fig. 13c. Increasing the rotational speed Ω sequentially, the gear system turns into period-two state from the chaos motion, and finally converges to the period-one motion, as seen in Figs. 16 and 17. Overall, it could be clearly observed from Figs. 8, 9, 10, 11, 12, 13, 14, 15, 16 and 17 that the dynamic load F_k of the system under chaotic motion is generally larger than that under period motion, which could deteriorate the dynamic responses of system. In addition, when rotational speed Ω changes, the meshing state of gear pairs only has no impact and single-sided impact, except the double-sided impact. It is thus imperative to choose the suitable parameter to control the motion state of the system and then reduce the vibration and avoid the chaos.

3.3 Effect of damping ratio ζ on bifurcation and chaos characteristics

To study the influence of damping ratio ζ on the dynamic behaviors, the damping ratio ζ is selected as the varying parameter in the corresponding bifurcation diagram and 3-D frequency spectrum. The other parameters of the system used in the next numerical simulation are as follows: $\mu = 0.07$, $\Omega = 1$, $b = 1$ and $F_m/F_a = 0.5$ or 2. Thus, Figs. 18 and 19 illustrate the bifurcation diagrams and 3-D frequency spectrums of the gear system under lightly and heavily loaded conditions, in which damping ratio ζ is under the range of $0 < \zeta < 0.2$.

As seen in Fig. 18a, under lightly loaded condition, the gear system shows diverse motion states including period-one, multi-period and chaotic motions. Therefore, it is indispensable to determine motion state of system in detail by using time-domain waveform, frequency plot, phase diagram, Poincaré map and dynamic load. When $\zeta > 0.17$, the time-domain waveform is periodic sinusoid, frequency plot has an amplitude peak, the phase diagram is an approximate ellipse, and the Poincaré map occurs a single point. The result indicates that the gear system is in period-one motion. The corresponding dynamic load is zero but has no negative value, where there exists single-sided impact when meshing. As damping ratio ζ is decreased, the system bifurcates into period two in the interval of $0.07 < \zeta < 0.17$. For instance, when $\zeta = 0.15$, the time-domain waveform is period-two harmonic response, frequency plot shows harmonics frequencies including 0.5Ω and 1.5Ω, the phase diagram is a non-circular closed curve and the Poincaré map has two discrete points, which can be observed from Fig. 21a–c. When ζ is 0.115 around, there appears jump discontinuity phenomena, where the vibration displacement changes abruptly whereas the system is also in the state of period two. Further decreasing damping ratio ζ, the gear system goes into period-four motion, even turns into period-eight motion. When ζ is equal to 0.068, the Poincaré map is four discrete points, revealing that system motion is period four, as shown in Fig. 22c. Similarly, under $\zeta = 0.061$, the Poincaré map in Fig. 23c is eight discrete points and the complex frequencies about $\Omega/4$, $\Omega/2$, $3\Omega/4$, Ω, $5\Omega/4$, $3\Omega/2$ appear in frequency diagram. These mean that the system is in period-eight motion. Finally, the gear system displays under the chaotic motion in the range of $\zeta < 0.058$. As $\zeta = 0.05$, the time-domain waveform is non-periodic curve, there are continuous and different frequency components in frequency plot, many disordered curves occur in the phase diagram, and the Poincaré map has lots of discrete points, as shown in Fig. 24a–c. When damping ratio ζ decreases, the dynamic loads have zero value among Figs. 20d, 21d, 22d, 23d and 24d, indicating that the system is always in the single-sided impact state (state II), while the amplitude of dynamic load increases gradually. In other words, as the damping ratio ζ is chosen to the smaller

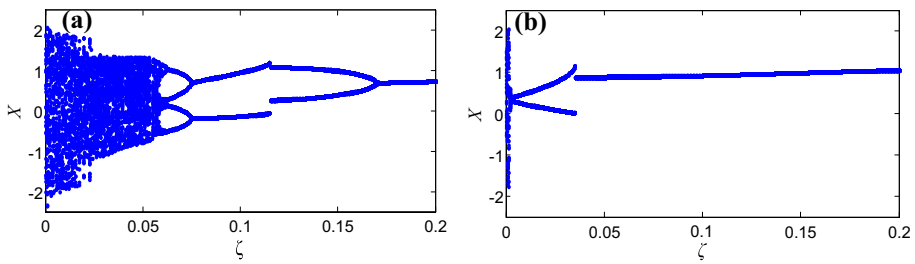

Fig. 18 Bifurcation diagrams with the varying of ζ under lightly and heavily loaded conditions, respectively

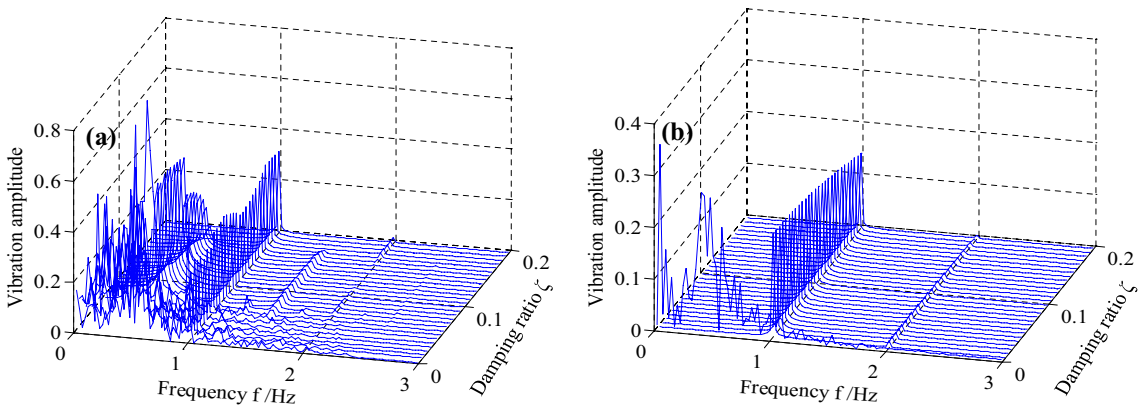

Fig. 19 3-D frequency spectrum with the varying of ζ under lightly and heavily loaded conditions, respectively

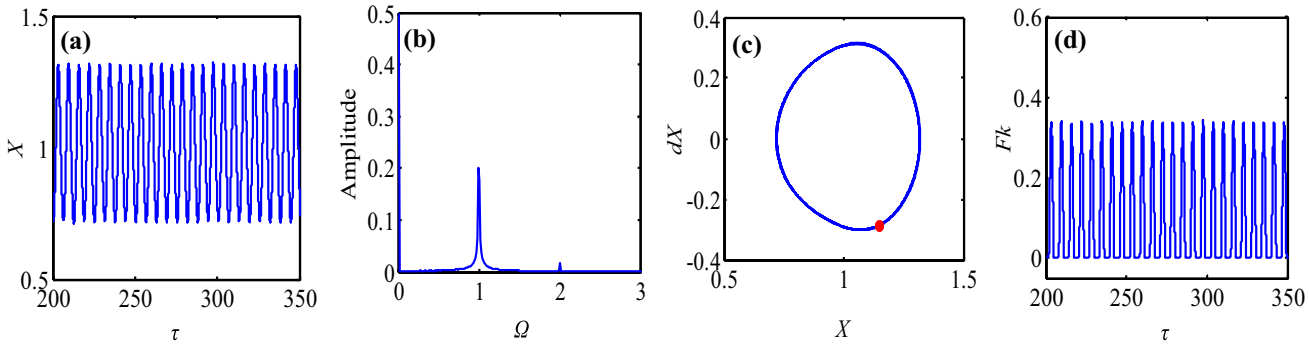

Fig. 20 Dynamic response curve at $\zeta = 0.19$. **a** Time-domain waveform, **b** frequency plot, **c** phase diagram and Poincaré map, **d** dynamic load

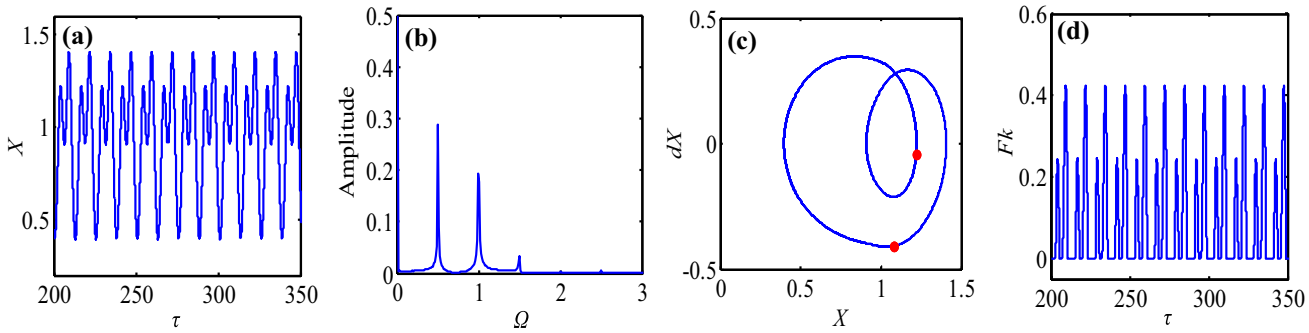

Fig. 21 Dynamic response curve at $\zeta = 0.15$. **a** Time-domain waveform, **b** frequency plot, **c** phase diagram and Poincaré map, **d** dynamic load

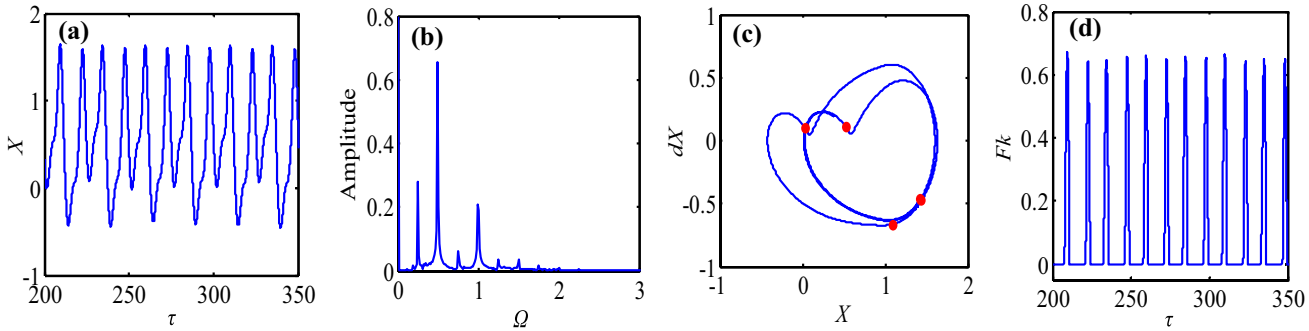

Fig. 22 Dynamic response curve at $\zeta = 0.068$. **a** Time-domain waveform, **b** frequency plot, **c** phase diagram and Poincaré map, **d** dynamic load

value, the dynamic load largens. Apparently, there exists the similar change trend of vibration amplitude as can be seen in frequency plot. However, as damping ratio ζ decreases further, the dynamic load has a negative value, which exhibits that the state of meshing gear pairs turns from single-sided impact into double-sided impact in Fig. 25 and could aggravate the dynamic characteristic of system.

From Fig. 18b, the period motions are the main motion responses of system in range of $0 < \zeta < 0.2$ under the heavily loaded condition. It should be pointed out that the system is in the chaotic motion only at very low values of damping ratio ζ, where there appear continuous and complex frequencies observed from the corresponding 3-D frequency spectrum. Hence, it clearly shows that the dynamic behaviors of system are more complex under the condition of light load than under the condition of heavy load. Partly, it is due to the fact that the static meshing force will increase as well with the increase of external load and the contact states consisting of double-sided and single-sided impacts may disappear gradually and then make gear pair meshing continuously.

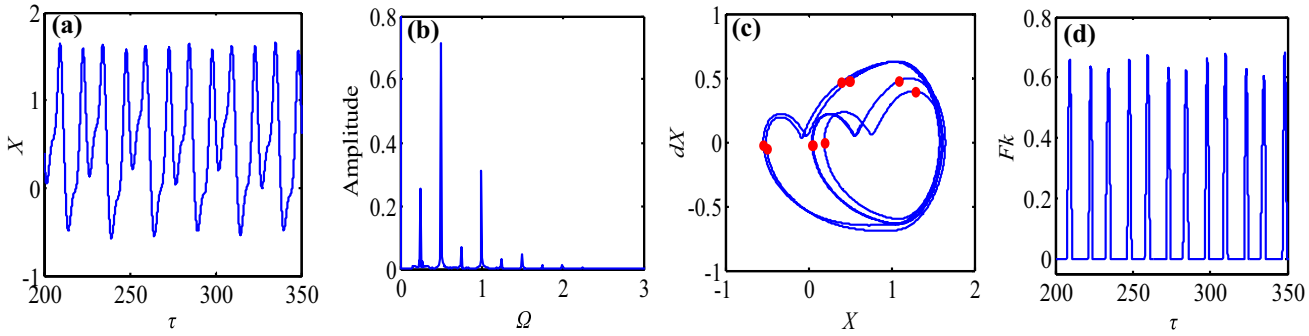

Fig. 23 Dynamic response curve at $\zeta = 0.061$. **a** Time-domain waveform, **b** frequency plot, **c** phase diagram and Poincaré map, **d** dynamic load

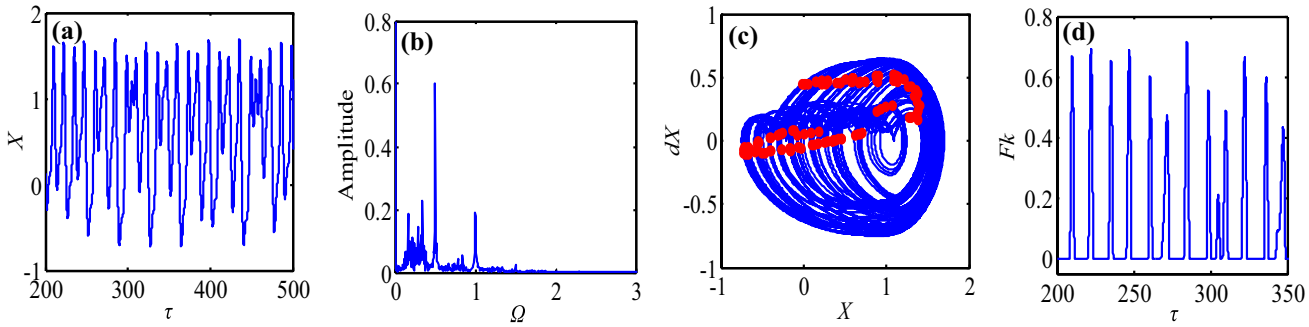

Fig. 24 Dynamic response curve at $\zeta = 0.05$. **a** Time-domain waveform, **b** frequency plot, **c** phase diagram and Poincaré map, **d** dynamic load

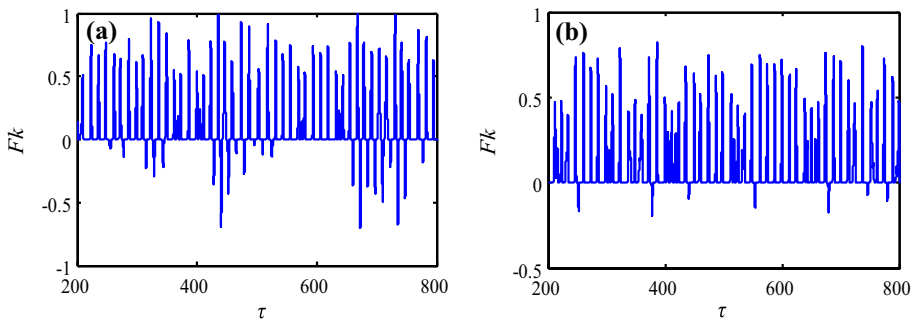

Fig. 25 Dynamic loads at $\zeta = 0.01, 0.03$

Through above analysis, as damping ratio ζ decreases from 0.2 to 0, the gear pair starts with period-one state, and then goes through multi-period motion, i.e. period-two, period-four and period-eight, and finally bifurcates into chaotic motion. Keeping rotational speed, gear backlash and other parameters constant, it could enhance stability and reliability of the gear system as ζ increases, owing to the energy consumed by the power transmission.

3.4 Effect of gear backlash *b* on bifurcation and chaos characteristics

Considering manufacture and assembly errors, gear lubrication and so forth, there exists backlash all the time in gear system. The strong nonlinearity caused by gear backlash makes the meshing contact state of gear pair change frequently. Under single-sided impact, double-sided impact or alternate states between the above two impact forms, the system may be in violent vibration. Thus, it

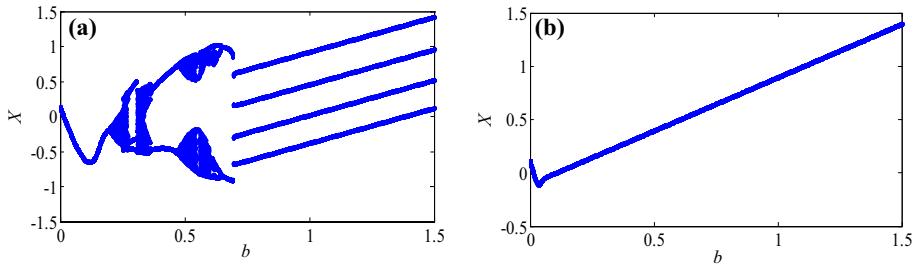

Fig. 26 Bifurcation diagrams with the varying of b with respect to X under lightly and heavily loaded conditions, respectively

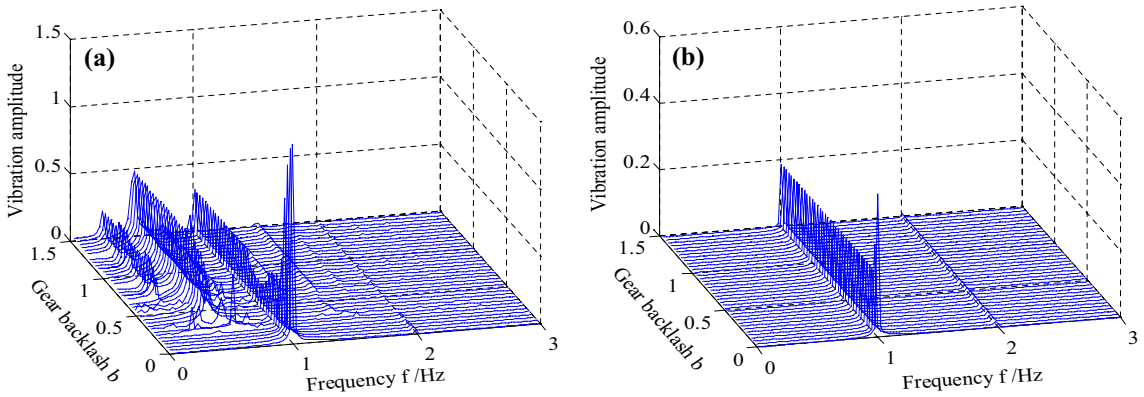

Fig. 27 3-D frequency spectrum with the varying of b under lightly and heavily loaded conditions, respectively

is vital to analyze the effect of gear backlash b on the dynamic behaviors of system.

In this subsection, the gear backlash b is selected as a control parameter in the bifurcation diagram and 3-D frequency spectrum. Meantime, the other parameters in the gear system are set as follows: $\zeta = 0.07$, $\Omega = 1$, $\mu = 0.07$ and $F_m/F_a = 0.5$ or 2. Then, the bifurcation diagrams and the corresponding 3-D frequency spectrums with the change of b under lightly and heavily loaded conditions, respectively, are illustrated in Figs. 26 and 27. Under lightly loaded condition, as gear backlash b increases, the gear system shows rich bifurcation features which contains period-doubling bifurcation, reverse bifurcation and so forth, indicating the system goes through complex motion states. However, under heavily loaded condition, with the increasing of b, the gear is always at period-one state, as shown in Fig. 26b. It means that gear backlash b does not affect the motion property and only changes the displacement amplitude of system.

Owing to the complexity of bifurcation character, it is inevitable to show clearly the evolution process about motion states of gear system under lightly loaded condition. Figure 28 exhibits the particular bifurcation diagram with the range of $0.1 \le b \le 0.7$. Time-domain waveform, phase diagram, frequency plot, Poincaré map and dynamic load diagram are used to interpret the dynamic behaviors of gear set. When $b < 0.2$, the time-domain waveform is a single periodic sinusoid, frequency plot exists an amplitude

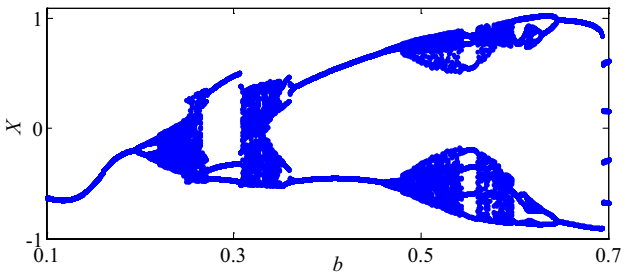

Fig. 28 Under lightly loaded condition, bifurcation diagram with the range of $0.1 \le b \le 0.7$

of excitation frequency, the phase diagram is sealed curve, and there is only a point in corresponding Poincaré map, as shown in Fig. 29a–c. The results represent the system undergoes period-one motion. The dynamic load alternately has a positive value and a negative value in Fig. 29d, indicating the meshing gear pair is under alternation states among no impact, single-sided impact and double-sided impact. However, in period motion, the system is subjected to severe tooth meshing states including tooth separation, tooth impact and large dynamic load, leading to the worse dynamic characteristic of system. Then, the system enters into the periodic doubling state, namely period-two and period-four forms. As gear backlash b keeps increasing, the system gets into chaotic motion in the scope of $0.22 < b < 0.27$.

When $b=0.25$, the time-domain waveform shows the non-periodic motion, the phase diagram becomes disorder, and the Poincaré map is evolved into the fractal structure, as shown in Fig. 30. These results mean the system is in the chaotic motion. However, the corresponding dynamic load is equal or lesser than zero in most of time of gear meshing process, which shows the meshing contact state of gear pair is under the state between single-sided impact and double-sided impact frequently alternately. After the width of chaotic motion region, the system bifurcates to period-three motion, as shown in Fig. 31. Comparing Fig. 31d with Fig. 30d, the time that dynamic load is greater than zero increases in Fig. 31d, which demonstrates no impact state appears frequently. Subsequently, the system enters into chaos motion again in the interval of $0.31<b<0.35$, where Fig. 32 illustrates the chaos state at $b=0.32$. As b increases further, the system gets into period-four motion. When $b=0.36$, the time-domain waveform shows the four periodic curve, and there are four discrete points in Poincaré map, as seen in Fig. 33a–c. The dynamic load still shows that the gear pair often switches meshing contact forms among the three impact states. And then, the gear system goes into period-two state by the route of reverse bifurcation. Keeping gear backlash b increasing further, the system

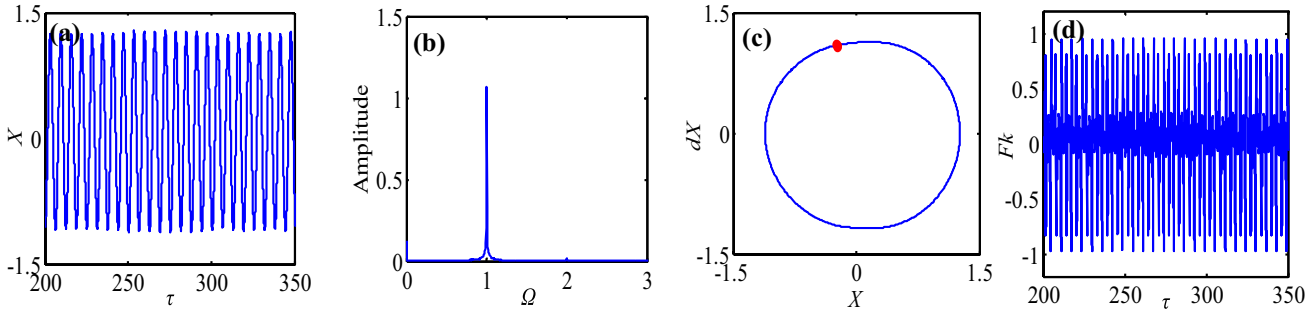

Fig. 29 Dynamic response curve at $b=0.1$. **a** Time-domain waveform, **b** frequency plot, **c** phase diagram and Poincaré map, **d** dynamic load

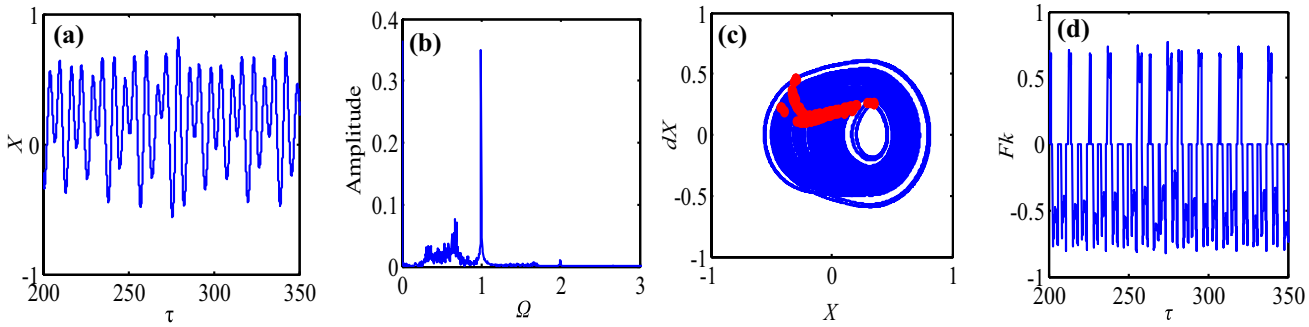

Fig. 30 Dynamic response curve at $b=0.25$. **a** Time-domain waveform, **b** frequency plot, **c** phase diagram and Poincaré map, **d** dynamic load

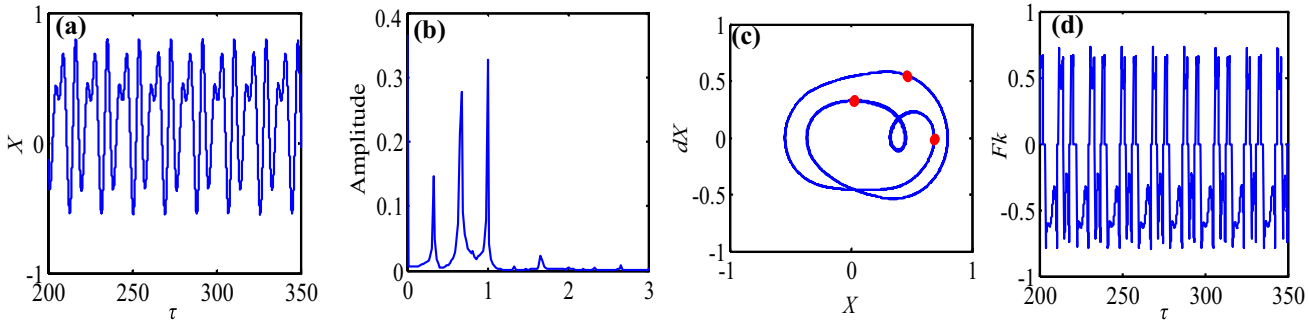

Fig. 31 Dynamic response curve at $b=0.28$. **a** Time-domain waveform, **b** frequency plot, **c** phase diagram and Poincaré map, **d** dynamic load

enters into the chaotic motion once more. When $b=0.53$, the time-domain waveform represents the non-periodic curve, the phase diagram is disorder and the Poincaré map is evolved into two fractal structures, as shown in Fig. 34a–c. Likewise, Fig. 34d suggests the meshing gear pair goes into severe contact states. Before getting into the next window of chaotic state, there exists a certain width of period-eight motion. When $b=0.55$, there are eight discrete points in Poincaré map in Fig. 35c, indicating the system is under the period-eight motion. Then, the gear system goes into the chaos motion, as shown in Fig. 36. Increasing the gear backlash b even further, the system gets back to the period motion. At $b=0.605$, the time-domain waveform, phase diagram and Poincaré map all show that the system enters period-four motion in Fig. 37. Then, the window of chaos motion appears again, as shown in Fig. 38. After the region of chaos, the gear pair bifurcates to period-four motion and then goes through period-two form, finally turns into period-four motion. When $b=1$, the corresponding dynamic load has the negative value no longer, as illustrated in Fig. 39. It means that the meshing contact of gear pair only has no impact state and single-sided impact state.

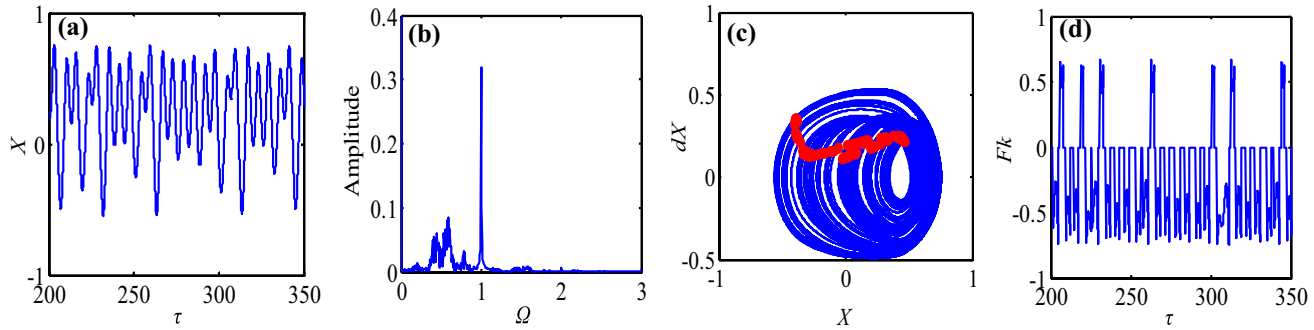

Fig. 32 Dynamic response curve at $b=0.32$. **a** Time-domain waveform, **b** frequency plot, **c** phase diagram and Poincaré map, **d** dynamic load

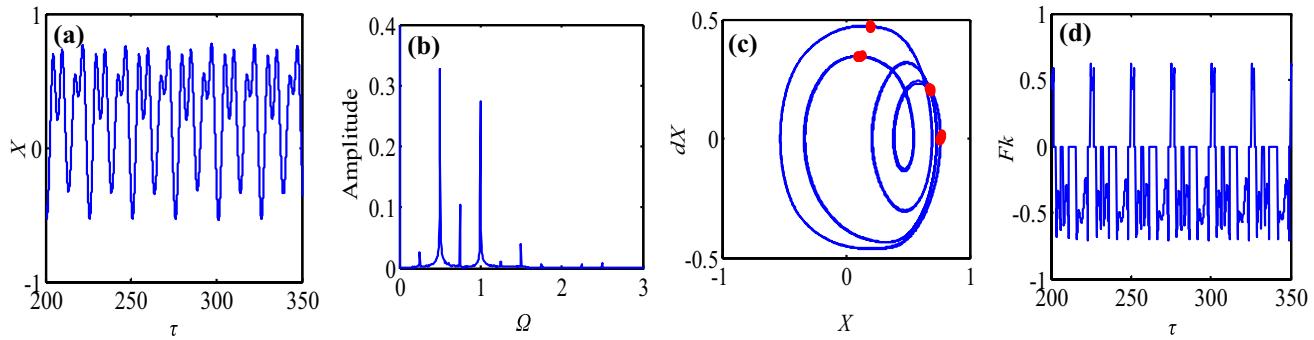

Fig. 33 Dynamic response curve at $b=0.36$. **a** Time-domain waveform, **b** frequency plot, **c** phase diagram and Poincaré map, **d** dynamic load

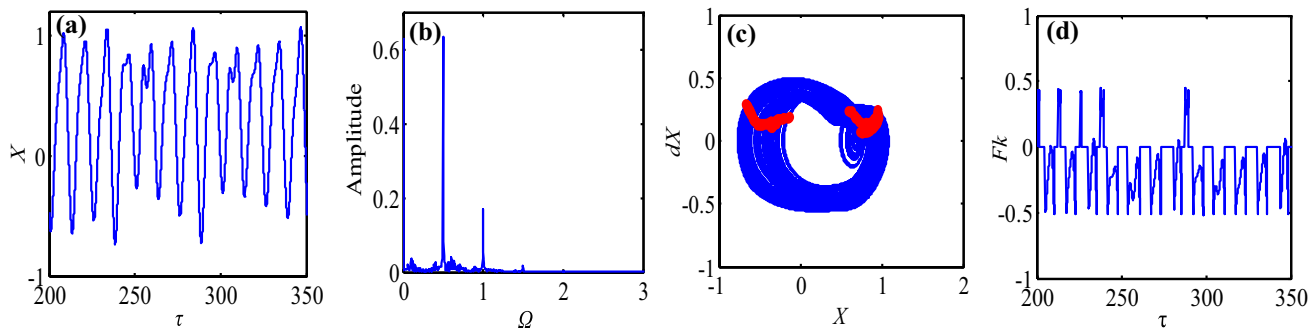

Fig. 34 Dynamic response curve at $b=0.53$. **a** Time-domain waveform, **b** frequency plot, **c** phase diagram and Poincaré map, **d** dynamic load

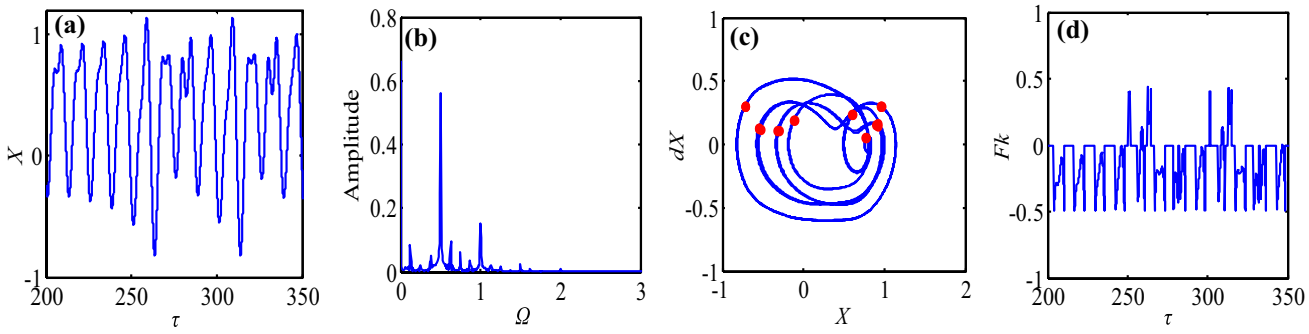

Fig. 35 Dynamic response curve at $b=0.55$. **a** Time-domain waveform, **b** frequency plot, **c** phase diagram and Poincaré map, **d** dynamic load

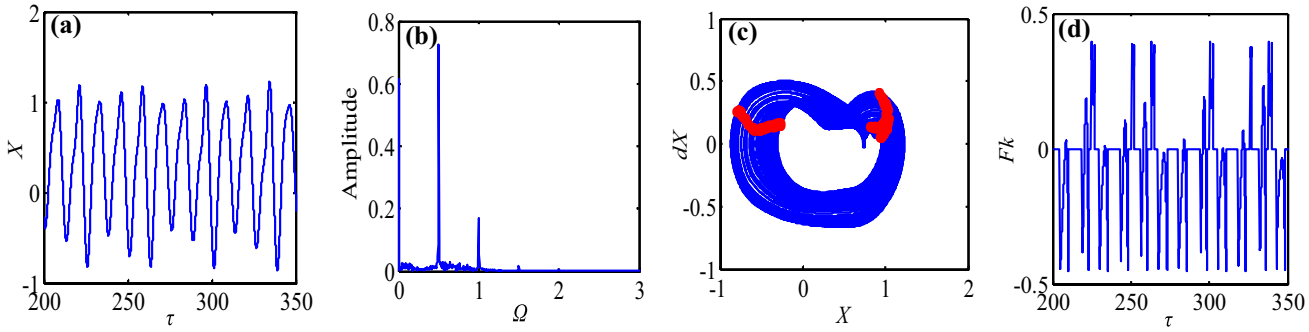

Fig. 36 Dynamic response curve at $b=0.586$. **a** Time-domain waveform, **b** frequency plot, **c** phase diagram and Poincaré map, **d** dynamic load

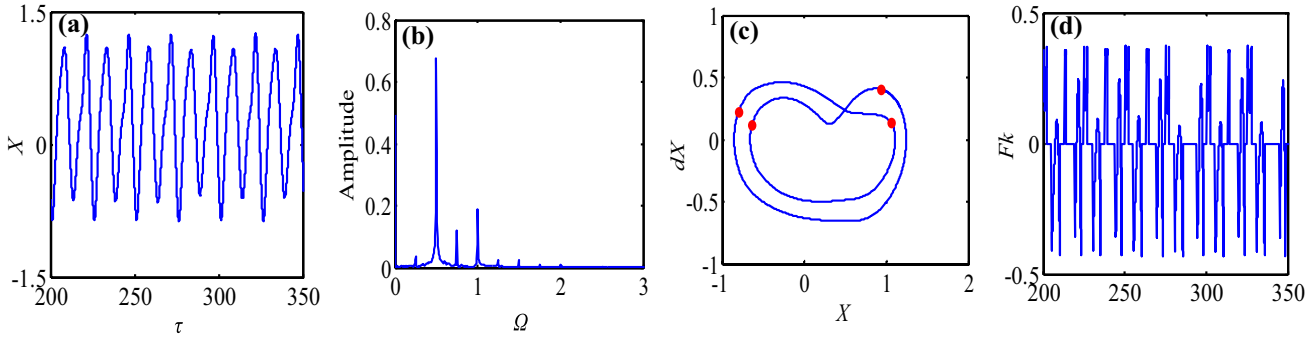

Fig. 37 Dynamic response curve at $b=0.605$. **a** Time-domain waveform, **b** frequency plot, **c** phase diagram and Poincaré map, **d** dynamic load

Based on the analysis above, it can be concluded that the varying gear backlash b gives rise to complex bifurcation features that the system goes through a diverse range of motion forms. In the chaotic state, the motions of system become unpredictable and uncontrollable. In addition, the dynamic load is high sensitivity to the change of gear backlash, which results in different impact states. Therefore, it is crucial to choose the suitable value of gear backlash for suppressing vibration of gear system, controlling impact state and avoiding chaos.

4 Conclusion

This paper builds a nonlinear dynamic model of a spur gear pair, which includes several nonlinear factors such as tooth face friction, static transmission error, backlash and time-varying stiffness. According to the extending period method, the time-varying meshing stiffness of gear pair is calculated. Meantime, the tooth face friction is derived based on the meshing principle. Then, the dynamic

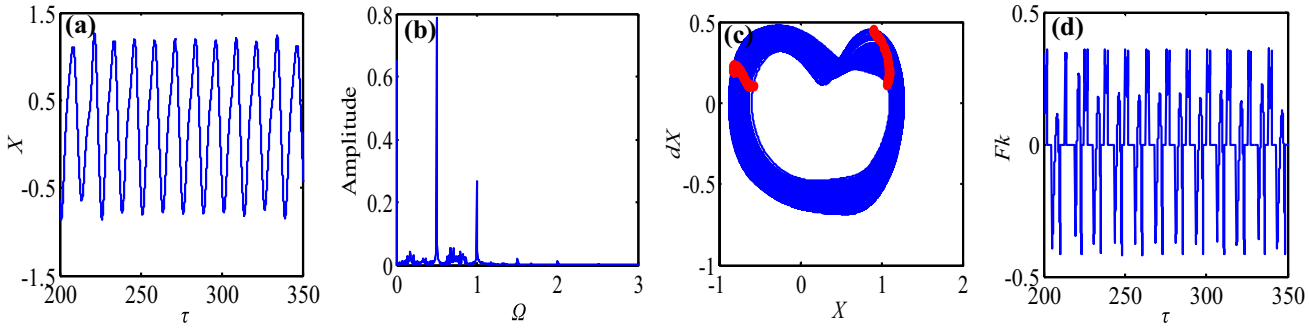

Fig. 38 Dynamic response curve at $b=0.618$. **a** Time-domain waveform, **b** frequency plot, **c** phase diagram and Poincaré map, **d** dynamic load

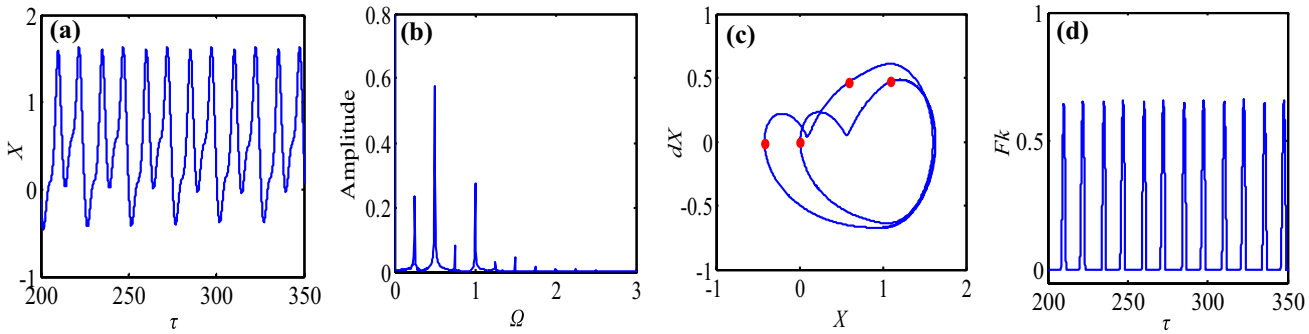

Fig. 39 Dynamic response curve at $b=1$. **a** Time-domain waveform, **b** frequency plot, **c** phase diagram and Poincaré map, **d** dynamic load

differential equation of the system is solved by applying Runge–Kutta numerical integration method. Rotational speed, damping ratio and backlash are selected as the control parameters to analyze the effect on the bifurcation and chaos characteristics under different loaded conditions. The dynamic responses of system are determined and discussed in detail from time-domain waveform diagram, frequency plot, phase portrait, Poincaré map and dynamic load diagram.

The analysis results show that as rotational speed increases under the condition of light load, the gear system initiates with periodic state, then goes through chaos, and lastly turns into the period motion again, showing rich motion forms. The corresponding meshing contact states are changed from no impact to single-sided impact state. However, under the condition of heavy load, the system only is in period motion including period-one and period double forms. Likewise, decreasing the damping ratio, the gear system turns into the chaotic motion via the channel of period double motion. The corresponding dynamic load is gradually increased with the decreasing of the damping ratio, where the meshing contact state of system is transferred from single-sided impact to double-sided impact. By contrast, when the gear system is under the condition of heavy load, the width of chaos region becomes narrow extremely, which is almost superseded by periodic motion. Besides, when gear backlash changes, there are several windows of the chaotic motion in bifurcation diagrams under lightly loaded condition. When gear backlash is smaller value, the dynamic load has a negative value, which means the meshing gear pair is in the state of double-sided impact. Whereas the system is always in period-one state with gear backlash increasing under heavily loaded condition. Overall, the nonlinear dynamic responses of gear system with friction are investigated in detail; especially, the proper values of system parameters should be chosen to reduce vibration amplitude, avoid the chaos and enhance the stability of system.

Though the bifurcation and chaos features for a spur gear pair system with sliding friction have been analyzed, there are some crucial topics that should be investigated in the future. Therefore, the stability analysis and the effect of friction on vibration displacement, chaos and bifurcation of gear system will be studied in the next stage.

Acknowledgements This work is supported by the National Natural Science Foundation of China (No. 51575320) and Taishan Scholar Foundation (TS20130922).

References

1. Xiang L, Nan G (2017) Coupled torsion–bending dynamic analysis of gear–rotor–bearing system with eccentricity fluctuation. Appl Math Model 50:569–584
2. Zhou S, Song G, Ren Z et al (2016) Nonlinear dynamic analysis of coupled gear–rotor–bearing system with the effect of internal and external excitations. Chin J Mech Eng 29(2):281–292
3. Kahraman A, Singh R (1990) Non-linear dynamics of a spur gear pair. J Sound Vib 142(1):49–75
4. Kahraman A, Singh R (1991) Non-linear dynamics of a geared rotor-bearing system with multiple clearances. J Sound Vib 144(3):469–506
5. Kahraman A, Singh R (1991) Interactions between time-varying mesh stiffness and clearance non-linearities in a geared system. J Sound Vib 146(1):135–156
6. Raghothama A, Narayanan S (1999) Bifurcation and chaos in geared rotor bearing system by incremental harmonic balance method. J Sound Vib 226(3):469–492
7. Theodossiades S, Natsiavas S (2000) Non-linear dynamics of gear pair systems with periodic stiffness and backlash. J Sound Vib 229(2):287–310
8. Al-Shyyab A, Kahraman A (2005) Non-linear dynamic analysis of a multi-mesh gear train using multi-term harmonic balance method: period-one motions. J Sound Vib 284:151–172
9. Al-Shyyab A, Kahraman A (2005) Non-linear dynamic analysis of a multi-mesh gear train using multi-term harmonic balance method: sub-harmonic motions. J Sound Vib 279:417–451
10. Shen Y, Yang S, Liu X (2006) Nonlinear dynamics of a spur gear pair with time-varying stiffness and backlash based on incremental harmonic balance method. Int J Mech Sci 48(11):1256–1263
11. Walha L, Fakhfakh T, Haddar M (2006) Backlash effect on dynamic analysis of a two-stage spur gear system. J Fail Anal Prev 6(3):60–68
12. Chang-Jian CW (2010) Strong nonlinearity analysis for gear bearing system under nonlinear suspension—bifurcation and chaos. Nonlinear Anal Real World Appl 6(3):1760–1774
13. Farshidianfar A, Saghafi A (2014) Global bifurcation and chaos analysis in nonlinear vibration of spur gear systems. Nonlinear Dyn 75(4):783–806
14. Farshidianfar A, Saghafi A (2014) Bifurcation and chaos prediction in nonlinear gear systems. Shock Vib 2014:1–8
15. Zhao M, Ji J (2015) Nonlinear torsional vibrations of a wind turbine gearbox. Appl Math Model 39(16):4928–4950
16. Wang J, He G, Zhang J et al (2017) Nonlinear dynamics analysis of the spur gear system for railway locomotive. Mech Syst Signal Process 85:41–55
17. Gou X, Zhu L, Qi C (2017) Nonlinear dynamic model of a gear–rotor–bearing system considering the flash temperature. J Sound Vib 410:187–208
18. Liu Z, Liu Z, Zhao J et al (2017) Study on interactions between tooth backlash and journal bearing clearance nonlinearity in spur gear pair system. Mech Mach Theory 107:229–245
19. Howard I, Jia S, Wang J (2001) The dynamic modelling of a spur gear in mesh including friction and a crack. Mech Syst Signal Process 15(5):831–853
20. Vaishya M, Singh R (2001) Analysis of periodically varying gear mesh systems with coulomb friction using Floquet theory. J Sound Vib 243(3):525–545
21. Vaishya M, Singh R (2001) Sliding friction-induced non-linearity and parametric effects in gear dynamics. J Sound Vib 248(4):671–694
22. He S, Cho S, Singh R (2008) Prediction of dynamic friction forces in spur gears using alternate sliding friction formulations. J Sound Vib 309:843–851
23. Wang J, Zheng J, Yang A (2012) An analytical study of bifurcation and chaos in a spur gear pair with sliding friction. In: International conference on advances in computational modeling and simulation. Kunming, Procedia Engineering, vol 31, pp 563–570
24. Chen S, Tang J, Luo C et al (2011) Nonlinear dynamic characteristics of geared rotor bearing systems with dynamic backlash and friction. Mech Mach Theory 46(4):466–478
25. Moradi H, Salarieh H (2012) Analysis of nonlinear oscillations in spur gear pairs with approximated modelling of backlash nonlinearity. Mech Mach Theory 51(5):14–31
26. Xiang L, Jia Y, Li Y et al (2016) Nonlinear dynamic features of a gear system with multi-DOF subjected to internal and external excitation. J Vib Shock 35(13):153–159 **(in Chinese)**
27. Liu X, Yang Y, Zhang J (2016) Investigation on coupling effects between surface wear and dynamics in a spur gear system. Tribol Int 101:383–394
28. Jiang H, Liu F (2017) Dynamic modeling and analysis of spur gears considering friction–vibration interactions. J Braz Soc Mech Sci Eng 39:4911–4920
29. Wang Y, Liu J, Li Y et al (2017) Parametric vibration stability of locomotive gear transmission system with tooth surface friction. J Traffic Transp Eng 17(2):52–63
30. Zhou S, Song G, Sun M et al (2018) Nonlinear dynamic response analysis on gear–rotor–bearing transmission system. J Vib Control 24(9):1632–1651
31. Sun Z, Shen Y, Li H (2003) Coexistence of trivial and strange attractors in star gear systems. J Vib Eng 16(2):242–246
32. Buckingham E (1949) Analytical mechanics of gears. Dover, New York
33. Sheng D, Zhu R, Jin G et al (2015) Dynamic load sharing behavior of transverse-torsional coupled planetary gear train with multiple clearances. J Cent South Univ 22:2521–2532